

Estimating the Effect of Satellite Orbital Error Using Wavelet-Based Robust Regression Applied to InSAR Deformation Data

Manoochehr Shirzaei and Thomas R. Walter

Abstract—Interferometric synthetic aperture radar data are often obtained on the basis of repeated satellite acquisitions. Errors in the satellite orbit determination, however, propagate to the data analysis and may even entirely obscure the interpretation. Many approaches have been developed to correct the effect of orbital error, which sometimes may even distort the signal. Phase contributions due to other sources, such as surface deformation, atmospheric delay, digital elevation model error, and noise, may reduce the accuracy of the orbital error estimation. Therefore, a more sophisticated approach for estimating the effect of orbital errors is required. In this paper, wavelet multiresolution analysis is employed to distinguish between the effects of orbital errors and other components (e.g., deformation signal). Next, a robust regression approach is applied to estimate the effect of orbit errors as a ramp. After describing the concept of this approach, we present a validation test using a synthetic data set. As in a real case study, the method is applied to an interferogram that was formed over the Tehran area in northern Iran. The validation test demonstrates that the orbital ramp can be estimated with a precision of 3 mm. Thus, a similar precision may be obtained in real cases such as the examined data set from over the Tehran area.

Index Terms—InSAR, orbital error, robust regression, wavelet analysis.

I. INTRODUCTION

DIFFERENTIAL interferometric synthetic aperture radar (InSAR) is a procedure wherein two overlapped radar images that have been acquired from similar viewing geometries are interfered, and the geometrical phase contributions using satellite orbital ephemeris and a reference digital elevation model (DEM) are subtracted [1]. The resulting interferogram contains information about ground displacement and contributions from DEM errors, atmospheric delay, and the effect of satellite orbit errors [1].

The satellite state vector error can be decomposed into an along-track, a cross-track, and a radial component [2]. The along-track component is usually taken into account once the two radar images are coregistered [2]. The cross-track and radial components both generate orbital fringes, the so-called phase ramp, which are often parallel to the satellite track. More-

over, variations in the radial and cross-track components of the orbital error during the SAR acquisition may also generate perpendicular fringes [2]. The orbital error causes an incorrect so-called flat-earth phase to be subtracted [2].

In order to reduce the effects of orbital error (for simplicity, “the effects of orbital error” is called “orbital error”), for the case of topography height estimation, tie points or ground-control points can be used to constrain the reference phase at certain points in each interferogram [2]–[4]. In order to apply this approach, one should ensure that the observations at the selected points are not tainted by any other contributions, such as atmospheric delay or ground motion; however, this assumption is usually violated, and therefore, this approach may lead to an incomplete correction.

Kohlhase *et al.* have suggested correcting the orbital error by tuning the trajectories of the satellite orbit [5]. In this approach, starting from a good estimate of the orbital trajectories (e.g., trajectories obtained from Delft University) and counting roughly parallel fringes in an interferogram, radial and across-track corrections to the initial trajectories can be obtained. This approach is applicable to coherent interferograms in which the orbital fringes are countable. Moreover, the interferograms should not be affected by significant DEM error and atmospheric delay, and thus, it may not be an appropriate approach for refining interferograms in mountainous or volcanic regions.

The next most widely used approach to deal with the orbital error is to estimate a planar phase ramp in the range and azimuth direction [1] using the following form:

$$\varphi^{\text{orbit}}(\eta, \xi) = a + b\eta + c\xi \quad (1)$$

where η and ξ are the azimuth and range in the radar coordinate system, respectively. The unknowns a , b , and c can be estimated using the least square (LSQ) method [6]; however, in cases where no other component contributes to the interferometric phase, a quadratic approximation performs better, particularly for DEM generation [2]. In the likely case of an unknown signal with a spatial scale comparable to the orbital error, applying a quadratic approximation may distort the signal.

The phase observation at a pixel that is located at the radar coordinates of (η, ξ) in an interferogram can be formulated as follows [2]:

$$\begin{aligned} \varphi^{\text{int}}(\eta, \xi) = & \varphi^{\text{def}}(\eta, \xi) + \varphi^{\text{atm}}(\eta, \xi) \\ & + \varphi^{\text{topo}}(\eta, \xi) + \varphi^{\text{orbit}}(\eta, \xi) + \varphi^n(\eta, \xi) \quad (2) \end{aligned}$$

Manuscript received April 30, 2010; revised October 21, 2010 and March 6, 2011; accepted March 20, 2011.

M. Shirzaei is with the Berkeley Seismological Laboratory, University of California, Berkeley, CA 94720 USA, and also with the Department 2: Physics of the Earth, GFZ German Research Centre for Geosciences, 14473 Potsdam, Germany.

T. R. Walter is with the Department 2: Physics of the Earth, GFZ German Research Centre for Geosciences, 14473 Potsdam, Germany.

Digital Object Identifier 10.1109/TGRS.2011.2143419

where φ^{def} , φ^{atm} , φ^{topo} , φ^{orbit} , and φ^n are the surface motion, atmospheric delay, DEM error, orbital error, and noise, respectively.

LSQ estimation of the orbital error using a planar ramp (1) is valid only if the other terms of (2) behave randomly [6]; however, in practice, this condition is often not fulfilled.

In this paper, a new approach to reliably estimate the planar phase ramp in an unwrapped interferogram that is contaminated by atmospheric delay, topographic error, and decorrelation noise subject to a high deformation rate is presented.

II. METHOD

Consider an interferogram that has been corrected for the reference geometrical phase contribution and unwrapped to obtain unambiguous phase values. Our approach to correct the effect of orbital error consists of two major steps: wavelet multiresolution analysis and robust regression. The first step aims to classify the spatial components of the unwrapped phase into short and long wavelength contributions. The assumption is that the long wavelengths mostly represent the orbital error. The regression then estimates the longest wavelength component in a robust manner. The combination of these two steps may lead to an accurate estimate of the orbital error.

A. Wavelet Multiresolution Analysis

Assuming $\Theta(\zeta, \eta)$ to be the unwrapped version of the interferogram $\varphi(\eta, \xi)$ with a size of $p \times q$, it can be decomposed in the wavelet domain using a multiresolution analysis [7] as follows:

$$\begin{aligned} \Theta(\zeta, \eta) &= \sum_{i_x}^{p-1} \sum_{i_y}^{q-1} v_{i_x i_y} \Phi_{J i_x i_y}(\zeta, \eta) \\ &+ \sum_{j'}^{J-1} \sum_{i_x}^{p-1} \sum_{i_y}^{q-1} \sum_{\varepsilon}^3 w_{j' i_x i_y}^{\varepsilon} \Psi_{j' i_x i_y}^{\varepsilon}(\zeta, \eta) \\ &= A^J + \sum_{j'}^{J-1} \sum_{\varepsilon}^3 D_{\varepsilon}^{j'} \end{aligned}$$

$$\Psi_{j' i_x i_y}^{\varepsilon}(\zeta, \eta) = \begin{cases} \Psi_{j' i_x}^{\varepsilon}(\zeta) \cdot \Phi_{j' i_y}^{\varepsilon}(\eta), & \varepsilon = 1 \\ \Phi_{j' i_x}^{\varepsilon}(\zeta) \cdot \Psi_{j' i_y}^{\varepsilon}(\eta), & \varepsilon = 2 \\ \Psi_{j' i_x}^{\varepsilon}(\zeta) \cdot \Psi_{j' i_y}^{\varepsilon}(\eta), & \varepsilon = 3 \end{cases}$$

$$\Phi_{J i_x i_y}(\zeta, \eta) = \Phi_{J i_x}(\zeta) \cdot \Phi_{J i_y}(\eta) \quad (3)$$

$$\begin{aligned} w_{j' i_x i_y}^{\varepsilon} &= \langle \Theta(\zeta, \eta), \Psi_{j' i_x i_y}^{\varepsilon}(\zeta, \eta) \rangle \\ v_{j' i_x i_y} &= \langle \Theta(\zeta, \eta), \Phi_{j' i_x i_y}(\zeta, \eta) \rangle \end{aligned} \quad (4)$$

where Φ and Ψ are the smoothing and the mother wavelet functions, respectively, v and w are the smoothing and wavelet coefficients, respectively, J is the number of wavelet scales, $\langle \cdot, \cdot \rangle$ is the inner product operator, and A and D are the components with long and short wavelengths, respectively.

The purpose of this decomposition is to discriminate between components that contribute to the unwrapped phase. The orbital

error has a relatively long wavelength, which affects the entire interferogram [2], whereas the DEM error and decorrelation noise may have a much shorter wavelength with a different amplitude in comparison to the orbital error (see [2] and [8]). The situation for the surface displacement and atmospheric delay can be different because they may present a behavior that is similar to the orbital error; i.e., a nearly constant phase gradient. In order to resolve this problem, the examined area of the interferogram should be larger than the area that is affected by the surface deformation and long wavelengths of the atmospheric delay. Thus, artifacts with large wavelengths cause problems in decomposition when they affect the entire interferogram.

The number of levels for wavelet decomposition is specified such that the effective wavelet window size is roughly the maximum wavelength of the surface deformation, atmospheric delay, DEM error, and decorrelation noise. This maximum wavelength might be estimated either visually or based on *a priori* information. The effective window size is twice the root mean square radius ($rmsr$) of the wavelet function, which may be calculated using the following equation [9]:

$$\begin{aligned} rmsr &= \frac{1}{\|\Psi\|} \left[\int_{-\infty}^{+\infty} (x - x^*)^2 |\Psi(x)|^2 dx \right]^{1/2}, \quad x = \xi, \eta \\ x^* &= \frac{1}{\|\Psi\|^2} \int_{-\infty}^{+\infty} x |\Psi(x)|^2 dx \\ \|\Psi\| &= \left[\int_{-\infty}^{+\infty} |\Psi(x)|^2 dx \right]^{1/2} \end{aligned} \quad (5)$$

where $|\cdot|$ is the absolute value operator. Here, it is assumed that effective window is a square in two dimensions.

B. Robust Regression

The wavelet decomposition of the unwrapped phase and the subtraction of short wavelengths primarily leaves the contributions of the orbital error. Now, it might be possible to apply (1); however, the requirements of applying an LSQ approach might not be fulfilled for several reasons. For instance, the uncertainty of the *a priori* information that is needed for adjusting the wavelet effective window size may lead to an inaccurate multiresolution analysis. Moreover, the selected wavelet family may not provide a spectral resolution that is fine enough to classify and remove all of the short wavelength components. Therefore, the contributions of these remaining components may act as outliers and systematic errors; thus, the main assumption for LSQ estimation approaches, i.e., randomly distributed error, is not fulfilled [6]. As an alternative, a more robust approach, such as the L_1 -norm minimization, can be used [10]. Implementing the L_1 -norm approximation requires rigorous mathematical calculations that lead to a linear or quadratic programming problem using Gauss–Markov models [11], [12].

A simpler result like the implementation of the L_1 -norm approximation may be achieved through robust regression [13]. This approach employs the iterative weighted LSQ (ILSQ) with observation reweighting as a function (e.g., bisquare) of the residuals from the previous step [13]. The advantage is that this algorithm can reduce the weight of outliers following iterations.

Assuming that A^n remains after the n level decomposition of the unwrapped phase of size $p \times q$ and contains only longer wavelengths, the mathematical model can be expressed as (6), shown at the bottom of the page, where r^ε is the error that is associated with the components of A^n . The weighted LSQ solution for (6) is as follows [6]:

$$\widehat{X} = (B^T P B)^{-1} B^T P L \quad (7)$$

where $P_{pq \times pq}$ is a diagonal weight matrix, i.e., P_{ii} is defined as the i th diagonal component of P . Here, P is defined based on the interferometric coherence map as follows:

$$P = \text{Vec}(C) \left/ \sum_{p,q} C_{p,q} \right. \quad (8)$$

where C is the coherence map and Vec is an operator that generates a columnwise vector of size $pq \times 1$ by putting the columns of C under one another. The residuals for observations are $V = L - B\widehat{X}$. In order to start the ILSQ estimation, a new weighting function is defined

$$\begin{aligned} Q^j &= W^j P, \quad j = 1, 2, \dots \\ Q^0 &= P. \end{aligned} \quad (9)$$

The W^j is the weighting function and has a size that is similar to that of P after iteration j , which is defined here as the so-called Cauchy function following [14]

$$\begin{aligned} W_{ii}^j &= 1 \left/ \left(1 + \left(R_i^j \right)^2 \right) \right., \quad i = 1, 2, \dots, pq \\ R_i^j &= V_i^{j-1} \left/ \left(T \times \sigma_{j-1} \times \sqrt{1 - h_i} \right) \right. \\ \sigma_{j-1}^2 &= V^{j-1T} Q^{j-1} V^{j-1} / r \end{aligned} \quad (10)$$

where T is the tuning factor (here, 2.385 after [14]), r is the degrees of freedom, and h is the distance of the observation pixel from the mean value of the ξ and η axes [15]. The further from the mean a pixel is, the greater influence this observation pixel has on the fitted surface.

The updated parameters are obtained as follows:

$$\begin{aligned} \widehat{X}^j &= (B^T Q^j B)^{-1} B^T Q^j L \\ V^j &= L - B\widehat{X}^j. \end{aligned} \quad (11)$$

The statistical properties of this estimation are detailed in [16]. The procedure of calculating the new weight and updating the parameters is repeated until a predefined stopping criterion is reached. The stopping criterion used here is as follows:

$$\left| \widehat{X}^j - \widehat{X}^{j-1} \right| < \delta \quad (12)$$

where δ is a small number (e.g., 10^{-7}). When the optimum parameters are obtained, the plane $\widehat{a} + \widehat{b}\eta + \widehat{c}\xi$ is subtracted from A^n , and the unwrapped phase is reconstructed using (3). In this way, the component that is extracted is mostly likely due to the orbital error effect if the deformation signal and atmospheric delay are of a smaller spatial scale. In the following section, this approach is evaluated in a synthetic test.

III. SYNTHETIC TEST

As an analogy to the case study (Section IV), a synthetic scenario was generated with a spatial dimension of $100 \times 100 \text{ km}^2$ and a pixel size of $80 \times 80 \text{ m}^2$, which is equivalent to the ENVISAT interferogram that is generated using multilooking factors of 20 and 5 along the azimuth and range, respectively. The synthetic unwrapped phase is obtained as the superposition of the effect of four deflating point sources [17] at depths of 3, 5, 4, and 6 km and volume changes of -0.01 , -0.01 , -0.03 , and -0.04 km^3 , respectively, in an elastic half-space medium. To simulate a more realistic scenario, white noise with a standard deviation of 50° and colored noise that is representative of a random atmospheric delay (similar to those obtained for the Netherlands test site by [2]) were added. Fig. 1(a) shows the simulated interferogram. The orbital error was simulated using a planar phase ramp [Fig. 1(b)], and the final signal, which contains the large deformation amplitude, atmospheric delay, noise, and orbital error, is demonstrated in Fig. 1(c). The coherence map that was used for the synthetic test is a map of the real case study that is shown in Fig. 3(e), and the areas with coherences of less than 0.1 are masked out. As can be seen in Fig. 1(a), the spatial extent of the area that is subject

$$\begin{aligned} L_{pq \times 1} + r_{pq \times 1}^\varepsilon &= B_{pq \times 3} X_{3 \times 1} \\ L^T &= [A_{11}^n \ A_{12}^n \ \dots \ A_{1q}^n \ A_{21}^n \ A_{22}^n \ \dots \ A_{2q}^n \ \dots \ A_{p1}^n \ A_{p2}^n \ \dots \ A_{pq}^n] \\ B^T &= \begin{bmatrix} 1 & 1 & \dots & 1 & 1 & 1 & \dots & 1 & \dots & 1 & 1 & \dots & 1 \\ \eta_{11} & \eta_{12} & \dots & \eta_{1q} & \eta_{21} & \eta_{22} & \dots & \eta_{2q} & \dots & \eta_{p1} & \eta_{p2} & \dots & \eta_{pq} \\ \zeta_{11} & \zeta_{12} & \dots & \zeta_{1q} & \zeta_{21} & \zeta_{22} & \dots & \zeta_{2q} & \dots & \zeta_{q1} & \zeta_{q2} & \dots & \zeta_{pq} \end{bmatrix} \\ X^T &= [a \ b \ c] \end{aligned} \quad (6)$$

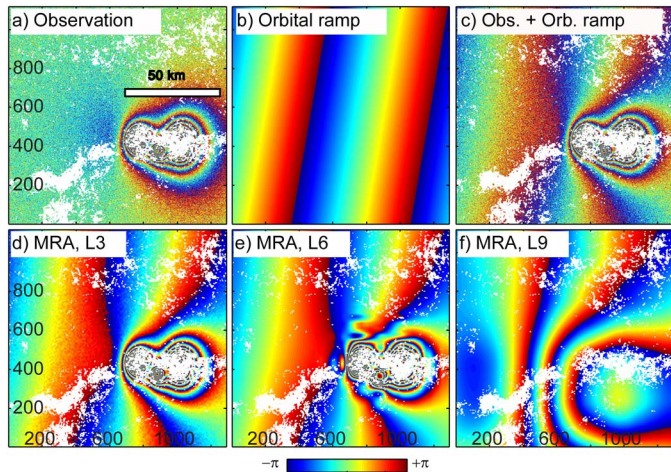


Fig. 1. Synthetic data set. (a) Simulated surface deformation using a superposition of the effect of four deflating point sources at depths of 3, 5, 4, and 6 km and volume changes of -0.01 , -0.01 , -0.03 , and -0.04 km^3 , including noise and random atmospheric delay. (b) Simulated orbital ramp. (c) Examined simulated interferogram including orbital ramp, deformation, and noise. (d)–(f) Wavelet decomposition at levels 3, 6, and 9. All panels are wrapped to the range $[-\pi, +\pi]$, and the white dots mark the location of the pixels with coherence below 0.1. (Obs) Observation. (Orb) Orbital. (MRA) Multiresolution analysis.

to large deformation is about 50 km, which is considered to be the maximum wavelength in the data set.

The multiresolution analysis was performed using Daubechies wavelet family of order 5 (db5) in nine levels of decomposition. The choice of wavelet family was empirically derived to achieve a balance between computation time and the wavelet support length that best fit the maximum spatial wavelength of the surface deformation, atmospheric delay, and phase noise. Other wavelet functions were also tested, such as Coiflet and Symlet, in addition to wavelet packets [18], and very similar results were obtained. In fact, wavelets apply low-pass filtering, and as long as a sufficiently fine spectral resolution is provided, any wavelet function can be used; however, identifying an optimum wavelet function requires a comprehensive numerical and theoretical analysis, which is beyond the scope of this paper and will be addressed in a dedicated study.

Fig. 1(d)–(f) shows the reconstructed low-frequency components (so-called “approximate”) at selected levels of 3, 6, and 9. The ILSQ approach is applied to the reconstructed signal at level 9 [Fig. 1(f)]. Following five iterations of ILSQ estimation, the stopping criterion was reached, and the corrected unwrapped phase that was obtained is presented in Fig. 2(a), with the residual (unwrapped phase–corrected phase) shown in Fig. 2(b). The signal that is associated with the surface deformation is retained while the orbital ramp is corrected. The orbital error, which has a root-mean-square error of 0.7 rad, remains after applying this correction, which is equivalent to ~ 3 -mm error in estimating the deformation field for the C-band ENVISAT mission. For comparison purposes, in Fig. 2(c)–(f), the results of applying conventional approaches [2] for the estimations of linear function (LF) and quadratic function (QF), respectively, are presented. As shown in Fig. 2(d) and (f), the conventional approaches, in this case, perform much worse than our novel technique. Therefore, the synthetic test demonstrates

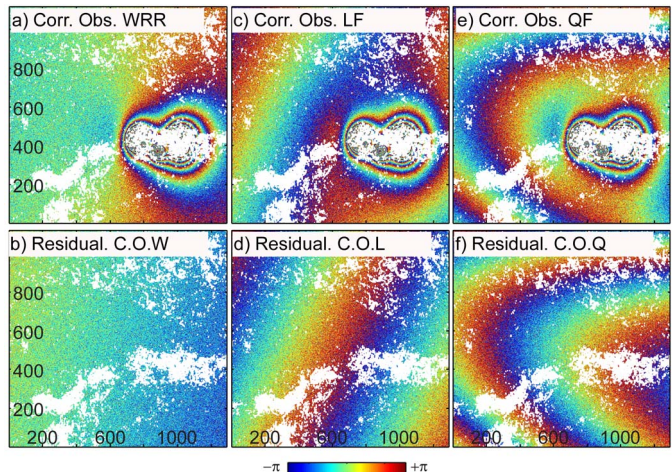


Fig. 2. (a) Corrected phase for the orbital ramp using our proposed method as a combination of wavelet analysis and robust regression. (b) Residual orbital ramp (unwrapped phase–corrected phase). (c) and (e) Corrected phase by applying conventional approaches using LF and QF. (d) and (f) Residual of the orbital ramp correction using LF and QF, respectively. All panels are wrapped to the range $[-\pi, +\pi]$, and the white dots mark the location of the pixels with coherence below 0.1. (Corr) Corrected. (Obs) Observation. (WRR) Wavelet-based robust regression. (LF) Linear function. (QF) Quadratic function. (C.O.W) Corrected observation by using wavelet robust regression. (C.O.L) Corrected observation by using linear function. (C.O.Q) Corrected observation by using quadratic function.

the merits of this approach for the reliable estimation of the orbital error.

In the next section, this approach is applied to an interferogram that was formed over an area of Tehran in northern Iran.

IV. CASE STUDY

A data set consisting of two radar images that were acquired by the ENVISAT radar satellite in a descending track over Tehran city, which is the capital of Iran and has ~ 13 million inhabitants, was used. The information of the interferogram is summarized in Table I. This interferogram maps one year of phase changes in the satellite line of sight. Fig. 3(a) shows the study area, and in Fig. 3(b), the geocoded interferogram is overlaid on a DEM, and the districts of Tehran city are marked by yellow lines. In the geocoded interferogram, several areas apparently undergo deformation in terms of concentrated fringes, which impact the western and southern parts of Tehran. Fig. 3(c)–(f) shows the interferometric phase, amplitude, coherence map, and unwrapped phase, respectively. Clearly, the area of the city exhibits high coherence and amplitude, whereas areas that are subject to rapid deformation or have mountains are poorly coherent.

Obviously, this interferogram encounters a high deformation rate with a relatively large spatial coverage, decorrelation processes, and an area that can be attributed to several phase fringes [seen in the upper left corner of Fig. 3(c)] that might partly or entirely be due to orbital error.

In order to correct the orbital error, the same procedure and parameters as those described in the simulated test were used. The stopping criterion was reached after seven iterations. For a direct comparison with the observed interferometric phase [Fig. 3(c)], the corrected phase was rewrapped, as shown in

TABLE I
INTERFEROMETRIC PARAMETERS OF THE PAIR
USED IN THE REAL CASE STUDY

Master acquisition date	2003.8.3
Salve acquisition date	2004.8.22
Master orbit	7446
Salve orbit	12957
Perpendicular base line	96 m
Doppler shift	-13.45 Hz

V. DISCUSSION

A new approach to correcting the effect of orbital error in repeat-pass interferometry that combines wavelet multiresolution analysis and robust regression was presented. Wavelet multiresolution analysis decomposes the signal into short and long wavelength components and, thus, may uncover the orbital error, which usually imposes long wavelength components. Furthermore, robust regression provides a reliable tool for estimating the orbital error as a ramp.

The wavelets are chosen because of their ability to deal with nonstationary signals (e.g., see [18] and [19]). The observed interferometric phase usually contains a variety of stationary and nonstationary components (e.g., local atmospheric turbulence), and dealing with them requires a more sophisticated algorithm, such as the wavelet transforms, which was adopted here. Another reason for this selection is that, for evaluating wavelet transform, it is not necessary to know the function values for the entire time/space axis; only the function at those axis values at which the wavelet is nonzero is needed. Consequently, an evaluation of the wavelet transform can be achieved in almost real time. This marvelous property satisfies future demands for real-time InSAR processing methods as a component of an early warning system for mitigating natural hazards, particularly when a larger number of radar satellites will provide very short revisit time acquisitions. However, when the contribution of nonstationary components is negligible and near real-time data handling is not required, other filtering approaches, such as Hanning windows [20], can be used.

The choice of db5 was empirically determined by testing various mother functions, which we identified to present a balance between efficiency and computation time in the synthetic and real case studies. In certain cases where wavelet decomposition does not provide a sufficiently fine spectral resolution, continuous wavelet decomposition or wavelet packets [18] can be used. These approaches, however, increase the computational load by an order of magnitude [9].

The major drawback of this approach is that the unwrapped phase is required. If the unwrapping step fails due to very low coherence and high phase noise, this approach is not applicable. Moreover, this approach is not capable of distinguishing between orbital errors and wide-scale atmospheric delays or deformation fields with very large spatial wavelengths and low rates. Moreover, the wavelet transform is applicable to regularly sampled data sets [18]. Thus, after removing low coherence pixels, the gaps were filled using a linear interpolation. Then, in the robust regression, the impact of these pixels was removed by fixing their weight to zero. In addition, several studies have applied wavelets to irregularly sampled data, which may avoid the uncertainties that result from the interpolation of data (e.g., [21]–[23]). Furthermore, because dyadic wavelets are used, the image is expanded by zeros to become a power of two. Robust regression attempts to find a solution that is less sensitive to outliers similar to those obtained by L_1 -norm minimization, and indeed, it succeeds if the initial weight is reasonably realistic. This paper demonstrates that coherence map-based weighting is a reasonable selection that guarantees the success of an algorithm.

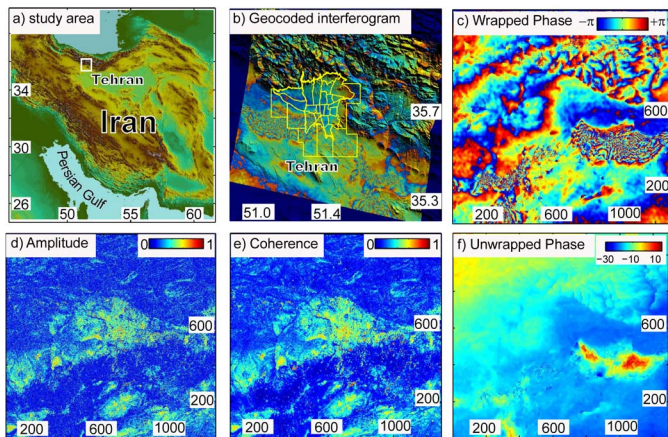


Fig. 3. Real case study over the Tehran plain. (a) Study area. (b) Geocoded interferogram overlaid on Shuttle Radar Topography Mission DEM, and the districts of Tehran city are marked by yellow lines. (c)–(f) Interferometric phase, amplitude, coherence map, and unwrapped phase, respectively.

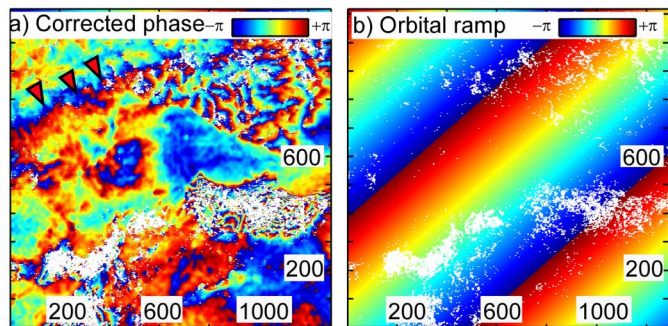


Fig. 4. (a) Corrected phase for the orbital ramp using the presented method in this paper. (b) Extracted orbital ramp. All panels are wrapped to the range $[-\pi, +\pi]$, and the white dots mark the location of the pixels with coherence below 0.1.

Fig. 4(a). Moreover, Fig. 4(b) presents the corrected orbital ramp. Obviously, when a ramp is corrected, most of the localized deformation is retained, and even other local effects become more visible [Fig. 4(a)]. As denoted in Fig. 4(a), a fringe that is similar to those generated by orbital error is also retained. By a comparison to Fig. 3(b) and (c), this fringe is located at the intersection of the mountain and the plain, which might have a different origin, such as ground displacement or atmospheric contributions.

Examining the synthetic cases, an accuracy of ~ 3 mm was achieved for the estimation of orbital error, which may behave randomly for independent pairs. Therefore, stacking several corrected interferograms or generating an InSAR time series (e.g., [24] and [25]) may result in a more significant reduction of the orbital error and lead to high-precision maps of the surface deformation field. The advantages of this approach are as follows: 1) it is applicable to very noisy data that contain large decorrelations (but phase unwrapping should still be possible); 2) it is applicable to data sets that are subject to large surface displacements and/or atmospheric delays; and 3) there is no need to have countable orbital fringes to identify the effects of orbital error contribution and direction.

VI. CONCLUSION

A novel approach to correcting the effects of orbital error in repeat-pass radar interferometry has been presented. The approach favors a combination of wavelet multiresolution analysis and robust regression for the estimation of the phase ramp that is induced by orbital error. Moreover, it is almost immune to DEM error, decorrelation noise, short wavelength, atmospheric delay, and high rates of surface deformation; despite the contributions of these components, it may still accurately estimate the orbital error. Our approach was tested and validated using synthetic and real data sets, and an orbital phase ramp estimation accuracy of ~ 3 mm was obtained. This approach can also be used to precisely identify slow tectonic processes using InSAR time series approaches.

ACKNOWLEDGMENT

The authors would like to thank B. Mansouri for providing the digital map of the districts of Tehran city.

REFERENCES

- [1] A. Ferretti, A. Monti-Guarnieri, C. Prati, F. Rocca, and D. Massonnet, *InSAR Principles: Guidelines for SAR Interferometry Processing and Interpretation*, K. Fletcher, Ed. Noordwijk, The Netherlands: ESA Publications, 2007, p. 48.
- [2] R. F. Hanssen, *Radar Interferometry, Data Interpretation and Error Analysis*. Norwell, MA: Kluwer, 2001.
- [3] D. Massonnet and K. L. Feigl, "Radar interferometry and its application to changes in the Earth's surface," *Rev. Geophys.*, vol. 36, no. 4, pp. 441–500, 1998.
- [4] P. Lundgren, E. A. Hetland, Z. Liu, and E. J. Fielding, "Southern San Andreas-San Jacinto fault system slip rates estimated from earthquake cycle models constrained by GPS and interferometric synthetic aperture radar observations," *J. Geophys. Res.*, vol. 114, pp. 1–18, 2009.
- [5] A. O. Kohlhase, K. L. Feigl, and D. Massonnet, "Applying differential InSAR to orbital dynamics: A new approach for estimating ERS trajectories," *J. Geodesy*, vol. 77, no. 9, pp. 493–502, 2003.
- [6] E. M. Mikhail, *Observations and Least Squares*. New York: IEP, 1976.
- [7] S. G. Mallat, "A theory for multiresolution signal decomposition: The wavelet representation," *IEEE Trans. Pattern Anal. Mach. Intell.*, vol. 11, no. 7, pp. 674–693, Jul. 1989.
- [8] Y. Gorokhovich and A. Voustianiouk, "Accuracy assessment of the processed SRTM-based elevation data by CGIAR using field data from USA and Thailand and its relation to the terrain characteristics," *Remote Sens. Environ.*, vol. 104, no. 4, pp. 409–415, Oct. 2006.
- [9] J. C. Goswami and A. K. Chan, *Fundamentals of Wavelets: Theory, Algorithms, and Applications*. New York: Wiley-Interscience, 1999.
- [10] H. Fuchs, "Contribution to the adjustment by minimizing the sum of absolute residuals," *Manuscripta Geodetica*, vol. 7, pp. 151–207, 1982.
- [11] J. Marshall and J. Bethel, "Basic concepts of L_1 norm minimization for surveying applications," *J. Surv. Eng.*, vol. 122, no. 4, pp. 168–179, Nov. 1996.
- [12] A. Amiri-Simkooei, "Formulation of L_1 norm minimization in Gauss-Markov models," *J. Surv. Eng.*, vol. 129, no. 1, pp. 37–43, Feb. 2003.
- [13] D. P. O'leary, "Robust regression computation using iteratively reweighted least-squares," *SIAM J. Matrix Anal. Appl.*, vol. 11, no. 3, pp. 466–480, Jul. 1990.
- [14] P. W. Holland and R. E. Welsch, "Robust regression using iteratively reweighted least-squares," *Commun. Statist.: Theory Methods*, vol. A6, pp. 813–827, 1977.
- [15] P. J. Rousseeuw and B. van Zomeren, "Unmasking multivariate outliers and leverage points," *J. Amer. Stat. Assoc.*, vol. 85, no. 411, pp. 633–639, Sep. 1990.
- [16] P. J. Huber, *Robust Statistics*. Hoboken, NJ: Wiley, 1981.
- [17] K. Mogi, "Relations between the eruptions of various volcanoes and the deformations of the ground surfaces around them," *Bull. Earthq. Res. Inst. (Tokyo)*, vol. 36, pp. 99–134, 1958.
- [18] I. Daubechies, *Ten Lectures on Wavelets*. Philadelphia, PA: SIAM, 1992.
- [19] W. Yuegang, X. Hongtao, and H. Teng, "Non-stationary signal denoising based on wavelet transform," in *Proc. IEEE ICEMI*, 2007, vol. 3, pp. 958–960.
- [20] R. L. Allen and D. Mills, *Signal Analysis: Time, Frequency, Scale, and Structure*. New York: Wiley-IEEE Press, 2004.
- [21] M.-S. Kim, S. Valette, H.-Y. Jung, and R. Probst, "Watermarking of 3-D irregular meshes based on wavelet multiresolution analysis," in *Proc. Int. Workshop Digital Watermarking*, vol. 3710, *Lecture Notes in Computer Science*, 2005, pp. 313–324.
- [22] W. Chen, S. Itoh, and J. Shiki, "Irregular sampling theorems for wavelet subspaces," *IEEE Trans. Inf. Theory*, vol. 44, no. 3, pp. 1131–1142, May 1998.
- [23] A. E. Milne and R. M. Lark, "Wavelet transforms applied to irregularly sampled soil data," *Math. Geosci.*, vol. 41, no. 6, pp. 661–678, Aug. 2009.
- [24] A. Ferretti, C. Prati, and F. Rocca, "Permanent scatterers in SAR interferometry," *IEEE Trans. Geosci. Remote Sens.*, vol. 39, no. 1, pp. 8–20, Jan. 2001.
- [25] P. Bernardino, G. Fornaro, R. Lanari, and E. Sansosti, "A new algorithm for surface deformation monitoring based on small baseline differential SAR interferograms," *IEEE Trans. Geosci. Remote Sens.*, vol. 40, no. 11, pp. 2375–2383, Nov. 2002.



Manoochehr Shirzaei was born in Zahedan, Iran, on September 21, 1981. He received the M.Sc. degree in geodesy from Tehran University, Tehran, Iran, and the Ph.D. degree (*summa cum laude*) from the University of Potsdam, Potsdam, Germany, in 2003 and 2010, respectively. He wrote his thesis on methods of InSAR time series analysis and time-dependent modeling of the source of volcanic and tectonic deformation fields.

In April 2011, he joined the Berkeley Seismological Laboratory, University of California, working on advanced algorithms for multitemporal interferometric processing of SAR data and crustal deformation field monitoring and modeling. His research interests are digital signal processing, remote sensing, and inverse theory.



Thomas R. Walter received the Ph.D. degree (*summa cum laude*) from the University of Kiel, Germany, in 2002.

As a Postdoctoral Researcher, he was with the InSAR lab at the Rosenstiel School of Marine and Atmospheric Science, University of Miami, Coral Gables, FL, from 2003 to 2005. Since then, he has been the Head of the Volcanology and Neotectonics Working Group, Department of the Physics of the Earth, GFZ German Research Centre for Geosciences, Potsdam, Germany. He is a Lecturer with the University of Potsdam, Potsdam, where he wrote his professorial thesis and also defended his habilitation in 2010.